



OPEN

Investigation of the motion of fullerene-wheeled nano-machines on thermally activated curved gold substrates

Mohammad Ali Bakhtiari, Saeed Seifi, Mahdi Tohidloo & Amir Shamloo

The current study presents one of the first investigations in which the simultaneous effect of the curved gold substrates and temperature changes on C_{60} and C_{60} -wheeled nano-machines' migration was evaluated. For this aim, the cylindrical and concave substrates with different radii were chosen to attain the size of the most appropriate substrate for nano-machines. Results indicated that the chassis' flexibility substantially affected the nanocar's mobility. Nano-machines' deviation from their desired direction was adequately restricted due to selected substrate geometries (The cylindrical and concave). Besides, for the first time, the effect of the substrate radius changes on nano-machine's motion has been investigated. Our findings revealed that adjusting the value of radius results in a long-range movement for nano-machines as well as a sufficient amount of diffusion coefficient even at low temperatures (75 K or 150 K). As a result, the aforementioned substrates could be utilized as the optimized geometries for C_{60} and nanocar at all temperatures. At the same time, the nanotruck displayed an appropriate performance merely on the small cylindrical substrate ($radius = 17.5 \text{ \AA}$) at high temperatures (500 K and 600 K).

Abbreviations

RBMD	Rigid-body molecular dynamics
STM	Scanning tunneling microscopy
EAM	Embedded atom method
MM	Molecular mechanics
FCC	Face-centered cubic
RHF	Restricted Hartree–Fock
LAMMPS	Large scale atomic/molecular massively parallel simulator
VMD	Visual molecular dynamics

In recent years, with the dramatic development in nanotechnology, some researchers have shown strong attention to the manipulation of nano-scale materials. Numerous theoretical studies and experimental researches have been accomplished in association with these materials^{1–4}. A great number of methods are present for manipulating one molecule or a cluster of atoms on a surface⁵. However, there are some drawbacks to these methods contrasting with the performance of natural nano-manipulators^{6,7}. First and foremost, they are not capable of working on abundant particles simultaneously⁸, and also, they are several orders of magnitude greater than the manipulated payloads⁹. Therefore, inspired by the transportation of atoms and molecules in nature in which molecules are in the same order of magnitude (or even smaller), investigations have attempted to fabricate manipulators whose sizes are in the same order of the corresponding payloads^{9–11}.

Tour et al. succeeded in fabricating several molecular motors and machines, aiming to carry other nano-scale materials^{9,12,13}. Due to the resemblance between these molecular motors and real cars, researchers named these synthesized molecular machines as nanocars, nanotrucks, or similar names^{8,9,12,14,15}. In the prior models of nano-machines, three or four-wheeled nano-machines in which C_{60} was utilized as a wheel were fabricated significantly^{12,16,17}. C_{60} is a well-known molecule that quite a few experimental and computational studies were reported its motion on different substrates^{6,17,18}. Additionally, since all reported nanocars and nanotrucks employed with C_{60} fullerene wheels, it seems that the comparison between C_{60} and the nano-machines not only

School of Mechanical Engineering, Sharif University of Technology, Azadi Ave., Tehran, Iran. email: shamloo@sharif.edu

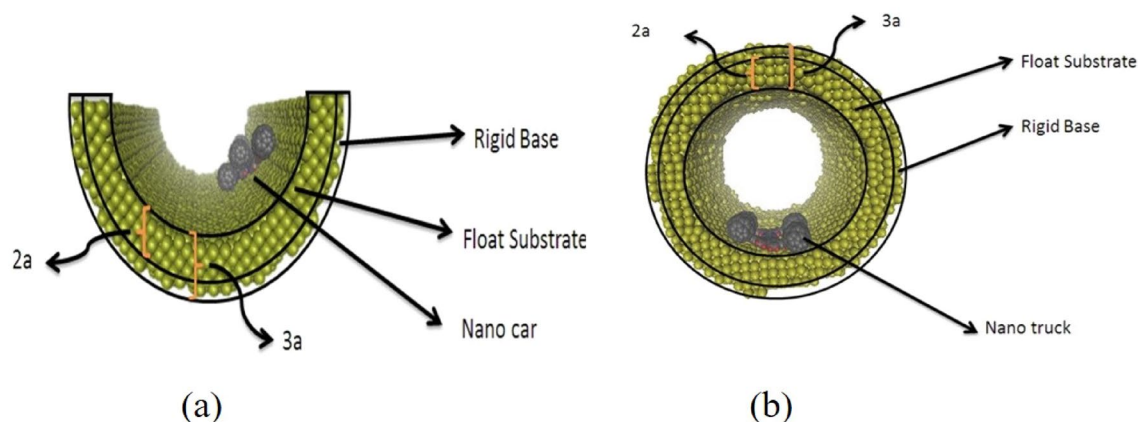


Figure 1. Description of simulation samples. **(a)** nanocar on the concave substrate and **(b)** nanotruck on the cylindrical substrate.

provides us with a better understanding of these machines, but may bring a breeding grounds for finding a correlation between them as well^{19,20}. Within the following generation, p-carborane-based wheels were extended in multiple nanocars concerning chassis with different shapes and even more wheels¹⁶. Besides, the small size of these nano-machines enabled them to be utilized in a considerable number simultaneously, which qualified them for transporting payloads effectively.

It should be noted that before using these nano-machines, it is necessary to determine their class of motion using experimental or analytical methods¹³. Scanning Tunneling Microscopy (STM) is a practical measuring method that monitors numerous types of nanocars²¹. Shirai et al.²² and Zhang et al.¹³ are two primary groups who investigated the motion of the nanocars' family using experimental studies. They analyzed the motion of several fullerene-wheel nanocars, at different temperatures, on a gold substrate. In addition, in some cases, they examined the effect of electric fields on nanocars' motion. It can be observed that using STM, few images were captured in a minute, and the details of the motion were partially displayed²³. In addition, STM suffers from several drawbacks, including being expensive and ridiculously time-consuming. Hence, it seems worthy to use computational simulation techniques, which are appropriate to measure the motion of these nano-structures in different conditions^{24–27}.

Nevertheless, a few kinds of fullerene-wheel nano-machines have been analyzed via computational simulation techniques so far. Akimov et al.²⁸ and Konyukhov et al.^{29,30} are two investigators who considered nanocars with rigid C_{60} wheels and rigid chassis. Although their simplifying assumptions allowed them to accomplish simulations more quickly, their model accuracy decreased drastically. In other words, by using rigid body molecular dynamics, the efficacy of chassis flexibility on the nanocar motion has been disassembled, and the chassis attachment to the substrate is not indicated properly. The issues mentioned above were solved by Nemati et al.³¹. They investigated the rotational and translational motions of nanocar and nanotruck on the gold substrate at different temperatures employing an all-atom model and classic atomistic dynamics to attain better accuracy. Their study helps us to better understand the thermally driven fullerene-based nano-machines with high controllability and maneuverability. Similarly, Mofidi et al. studied the motion of the C_{60} -wheeled nano-machines on the graphene substrates at different conditions and temperatures²⁵. They considered the diffusion coefficient of translational motion without taking into account the rotational motion, wheels, and chassis impacts on the mobility of nanocars. However, the motion of these nano-carriers on the curved shape substrate remains unexplored. For instance, gold nanotubes are recognized as outstanding nanomaterials with excellent load-carrying capacity and are malleable to different sizes and shapes³². Besides, In recent studies, gold nanotubes have been used as a promising candidate for multidisciplinary fields due to their specific features like large surface area, excellent adhesion properties, and corrosion resistance; some applications include electronic structure, biosensors, pharmaceuticals, and theranostic^{32–35}.

The current study presents one of the first investigations in which the simultaneous effect of the curved gold substrate and temperature changes on nano-machine migration were explored. The cylindrical and concave substrates were chosen as the curved substrate due to their similar contacting surface to the nano-machine wheels. In addition, these substrates can simultaneously simulate the motion of nano-machines on the flat, downward, and upward step substrates. In the first step, the impacts of chassis' attachment on the motion of nano-machines were also studied. Eventually, a correlation between the motion of the wheels, nanotruck, and nanocar on different substrate sizes was obtained.

Method

Potential energy approach. Potential energy analysis is an outstanding tool, enabling us to predict the regime of motion of a nanotruck or nanocar on the variant substrate conditions.

In this section, the potential energy of a C_{60} , nanocar, and nanotruck on curve-shaped gold substrates, comprised of a floating substrate (inner layer) and a rigid base (outer layer), has been investigated (Fig. 1). In addition, Fig. 2 shows the schematic views of a $3 \text{ nm} \times 4 \text{ nm}$ flexible-chassis nanocar and $2 \text{ nm} \times 3 \text{ nm}$ stiff-chassis

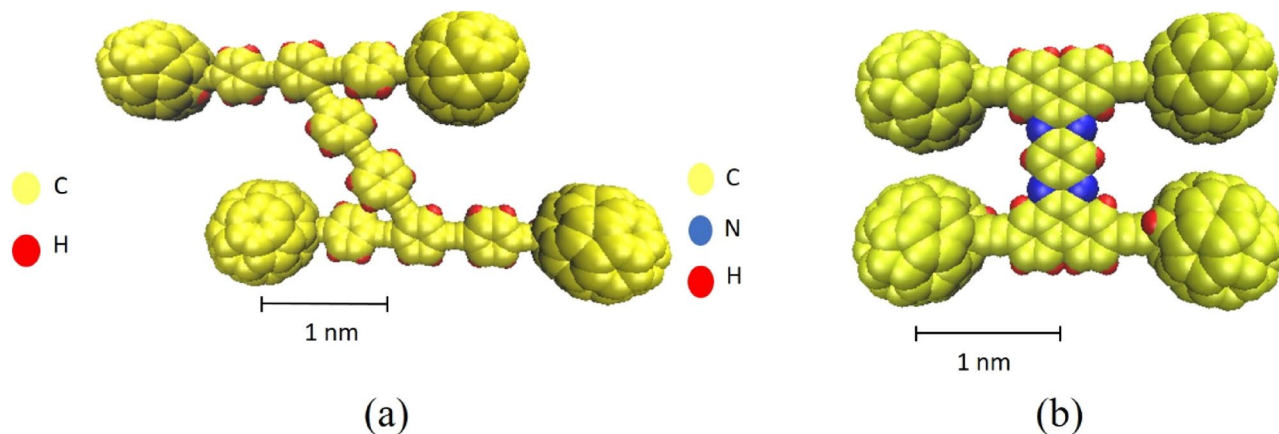


Figure 2. Top view of a fullerene-based molecular machine with four wheels: (a) Nanocar, the size of the exible-chassis machine is approximately 3 nm × 4 nm, (b) nanotruck, the chassis is practically rigid and due to the presence of nitrogen atoms in the chassis, it can potentially be attached to and carry other molecules. Its size is about 2 nm × 3 nm. In both molecules, the carbon, hydrogen, and nitrogen atoms are shown in gray, white, and blue, respectively.

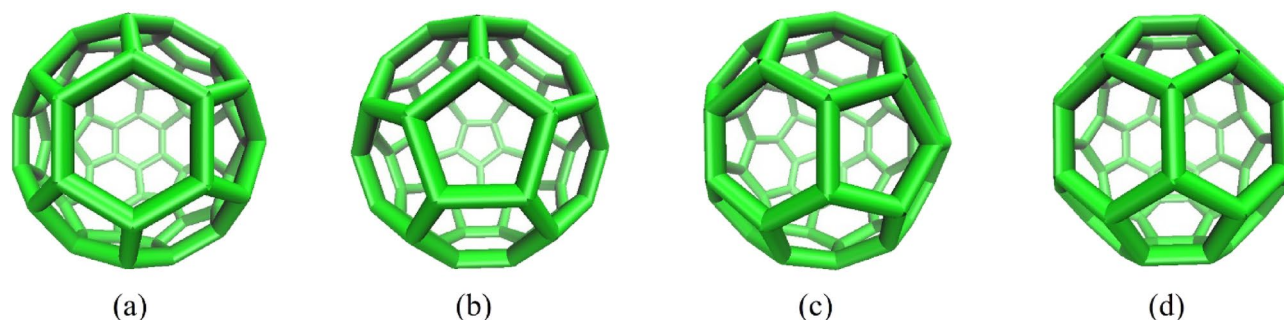


Figure 3. Orientations of C_{60} on gold surface (bottom view). (a) C_{60} on a hexagonal face (b) C_{60} on a pentagonal face (c) C_{60} on a bond between a pentagonal and a hexagonal faces (d) C_{60} on a bond between two adjacent hexagonal faces.

nanotrucks^{9–12}. As Pishkenari et al. reported²⁴, the orientation of C_{60} , nanocar, and nanotruck vigorously affected their potential energy on a gold substrate. They provided a comparison between four different C_{60} orientations, considering translational and rotational motion, and demonstrated that Hexa-down orientation has the most stable direction (Fig. 3).

Simulation setup. In the current study, the motion of C_{60} , nanocar, and nanotruck on the curved-shaped gold surfaces has been investigated using an atomistic dynamics approach. Simulations were performed at different temperatures in the range of 75 K to 600 K, considering various radii (17.5 Å to 30 Å for nonotruck and 20 Å to 30 Å for nanocar) on the curved surfaces. The minimum radius mentioned above, was considered for the geometries based on the size of C_{60} , nanocar, and nanotruck. Thus, the substrates with 20 Å and 17.5 Å radii were selected for nanocar and nanotruck, respectively. Besides, the gold nanotube has been stable at high temperatures; as the previous studies are highlighted at 900 K diffusion in the gold nanotube is intrusive, but atoms stick to the walls and do not move until 1200 K^{33,34,36,37}.

To evaluate the efficacy of temperature and radii on the mobility of C_{60} , the substrates' length was set to $27a$, where a stands for the gold lattice constant and assessed to be 4.078 Å³⁸. The nanocar or nanotruck was posited on the inner layer of gold substrates, while the outer layer was considered rigid. The embedded atom method (EAM) potential, which extended based on density functional theory, is able to predict dislocation structures well analogous with experimental observations³⁹. Thus, an EAM alloy potential, appropriate for modeling face-centered cubic (FCC) metals, and Molecular Mechanics (MM) force field was applied for modeling the interactions among the gold atoms and interaction within the nanotruck atoms, respectively^{40,41}. Considering the harmonic style, bonds and angles are formulated as below:

$$E_{bond} = K_b(r - r_0)^2 \quad (1)$$

$$E_{angle} = K_a(\theta - \theta_0)^2 \quad (2)$$

Bonds parameters				
$K_b (\frac{ev}{\text{\AA}^2})$	$r_0 (\text{\AA})$	Description		
48.6652	1.212	C2C2		
30.8837	1.313	C2CA		
25.1593	1.392	CACA		
14.3500	1.101	CAH		
34.5960	1.260	CANA		
Angles parameters				
$K_a (\frac{ev}{\text{rad}^2})$	θ_0	Description		
1.46619	π	C2C2CA		
1.34141	$2\pi/3$	C2CACA		
1.34141	$2\pi/3$	CACACA		
1.12304	$2\pi/3$	CACAH		
1.34141	$2\pi/3$	CACANA		
1.34141	0.638π	CANACA		
Dihedrals parameters				
$K_{d1} (ev)$	$K_{d2} (ev)$	$K_{d3} (ev)$	$K_{d4} (ev)$	Description
0	0.000043	0	0	CAC2C2CA
0	0.000043	0	0	C2C2CACA
0	0.650451	0	0	C2CACACA
0	0.650451	0	0	C2CACAH
-0.0403	0.208144	0	0	CACACANA
0	0.234379	0.046	0	CACACAH
0.0433	0.650451	0	0	CACACANA
0	0.390271	0	0	HCACAH
0	0.650451	0	0	HCACANA
0	0.433634	0	0	NACACANA
0	0.433634	0	0	CACANACA

Table 1. Parameters used in simulation of the nanocar and nanotruck.

In Eq. (1), K_b represents the bond stiffness, and r and r_0 stand for the bond distance and equilibrium bond distance, respectively. In addition, In Eq. (2), K_a is the angle stiffness, and θ and θ_0 are the angle and equilibrium angle, respectively⁴². Dihedral term style is presented in Eq. (3) as follows:

$$E_{dihedral} = \frac{1}{2}K_{d1}(1 + \cos\varphi) + \frac{1}{2}K_{d2}(1 - \cos2\varphi) + \frac{1}{2}K_{d3}(1 + \cos3\varphi) + \frac{1}{2}K_{d4}(1 - \cos4\varphi) \quad (3)$$

where φ is the dihedral angle and K_{d1} to K_{d4} represents the torsion stiffness parameters. The MM3 force field was performed to calculate the potential for these parameters, provided in Table 1, supposing that improper terms are negligible in the simulations^{43–47}. Simulations were performed using a Large scale Atomic/Molecular Massively Parallel Simulator (LAMMPS) solver⁴⁸, followed by visualizing the results on Visual Molecular Dynamics (VMD) software⁴⁹.

The substrate, the nanocar, and the nanotruck's temperature was controlled using two Nose–Hoover thermostats. The first principle theorem, i.e. Restricted Hartree–Fock (RHF), was utilized for calculating charge distribution in the nanocar and nanotruck molecules. Calculations were obtained by employing the NWChem 6.5 package and 6–31G** (d,p) basis set⁵⁰. Despite the fact that there is little charge distribution in the nanocar and nanotruck, in the light that the gold substrate is electrically neutral, charge transfer between the nano-machines and gold substrate was neglected. Therefore, the electric field does not affect the motion of nano-machines on the gold substrate^{51,52}.

In order to model the Van der Waals interactions between gold and carbon, hydrogen, and nitrogen atoms (C–Au, H–Au, and N–Au), Lennard–Jones 6–12 potential was utilized as:

$$E_{Lj} = 4\epsilon \left[\left(\frac{\sigma}{r} \right)^{12} - \left(\frac{\sigma}{r} \right)^6 \right] \quad (4)$$

where σ , ϵ , and r stand as potential parameters, representing the equilibrium distance, the well depth of the potential, and the distance between gold and carbon atoms at an equilibrium position, respectively. Table 2 summarizes the values for σ and ϵ parameters considering the same interaction parameters between gold and both types of carbon atoms (Fig. 4). Furthermore, the dimensions of the gold substrate in the horizontal and thickness orientations were considered large enough (three times the lattice constant), and the cut-off radius was set to $r_{cut-off} = 13 \text{ \AA}$ ($r_{cut-off} > 4\sigma$)⁵³.

ϵ (eV)	σ (Å)	Description
0.01273	2.994	C–Au
0.01315	2.611	H–Au
0.01423	2.886	N–Au
0.00190	3.460	C–C
0.00230	3.244	N–N
0.00204	2.673	H–H
0.00213	3.350	C–N
0.00197	3.647	C–H
0.00220	2.958	N–H

Table 2. Parameters of the Lj potential.

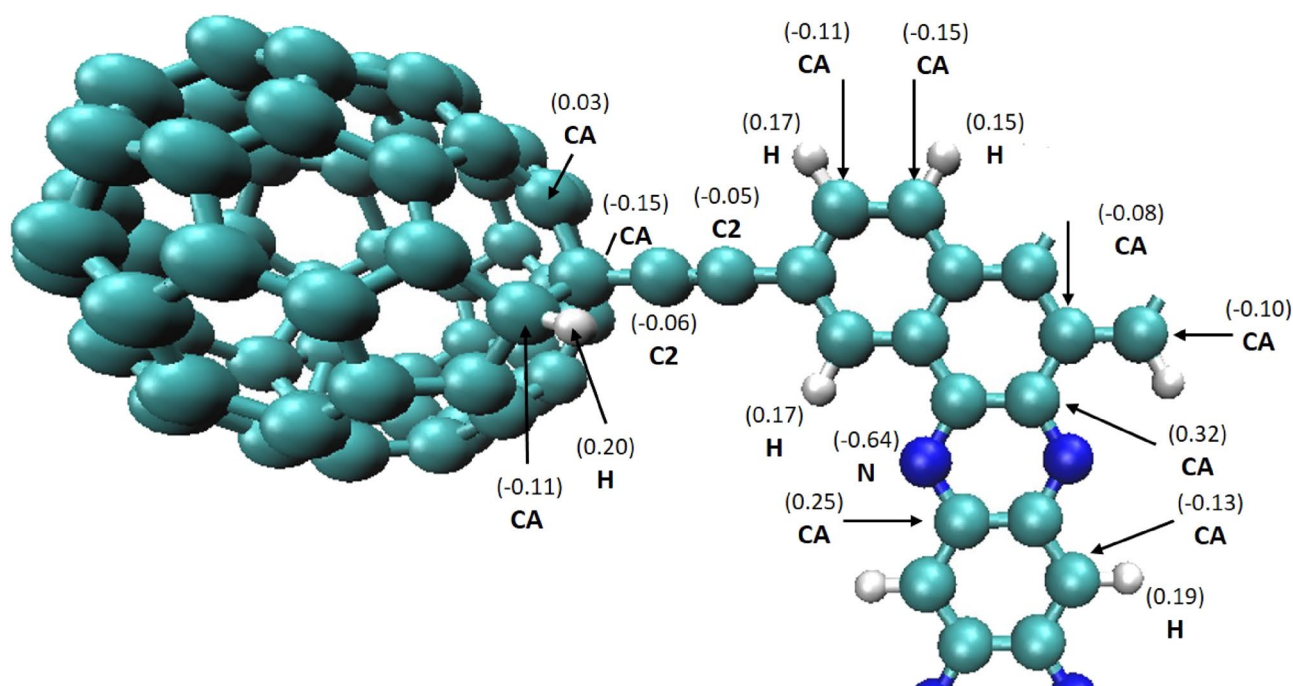


Figure 4. Different types of carbon atoms and charge distribution considered in the nanotruck.

Results and discussion

C₆₀. Figures 5 and 6 indicate the path of the C₆₀ molecule on the gold substrates in cylindrical and concave geometries, respectively. The motion of the C₆₀ molecule has less deviation from its direct pathway in the cylindrical geometry (Fig. 6). Likewise, this stability in motion was also observed in the concave-shaped substrates when the temperature and radii were increased (Fig. 5c–f). With increasing the radii, the number of gold molecules has increased, which decreases the substrate's surface-to-volume ratio. In other words, the surface effects were reduced, and as a result, the C₆₀ molecule moved approximately in a direct path. Increasing the temperature separately, does not always lead to direct motion of C₆₀ on substrates (e.g. Fig. 5c,f for $r = 30$ Å and Fig. 6c,f for $r = 30$ Å). To express the cause of this issue and understand the parameters affected by temperature and radius, the potential energy between the C₆₀ fullerene molecule and different gold substrates was investigated as well as changes in the diffusion coefficient (DC) of the C₆₀ molecule. The average potential energy and maximum potential energy diagrams of the C₆₀ molecule were represented in Figs. 7 and 8, respectively. As can be seen in both figures, the temperature changes over the mean and maximum potential energy at the same radii and geometry are almost negligible, which means that the adhesion between the C₆₀ and the gold surface does not differ when the temperature increases at the same radii. Hence, this parameter is not a cause for less mobility of C₆₀ in the aforementioned items (e.g., Fig. 5c,f for $r = 30$ Å, Fig. 6c,f for $r = 30$ Å). In addition, other results were obtained from Figs. 7 and 8, from which the average and maximum potential energy were increased, in the cylindrical substrate; it is twice as concave, with increasing radius in both geometries.

A diffusion coefficient diagram for the C₆₀ molecule at different radii and temperatures is presented in Fig. 9. The diffusion coefficient has been recognized as one of the essential characteristics in the motion of the C₆₀. Comparing the diffusion coefficient diagram and obtained results from Figs. 5 and 6, the higher value for

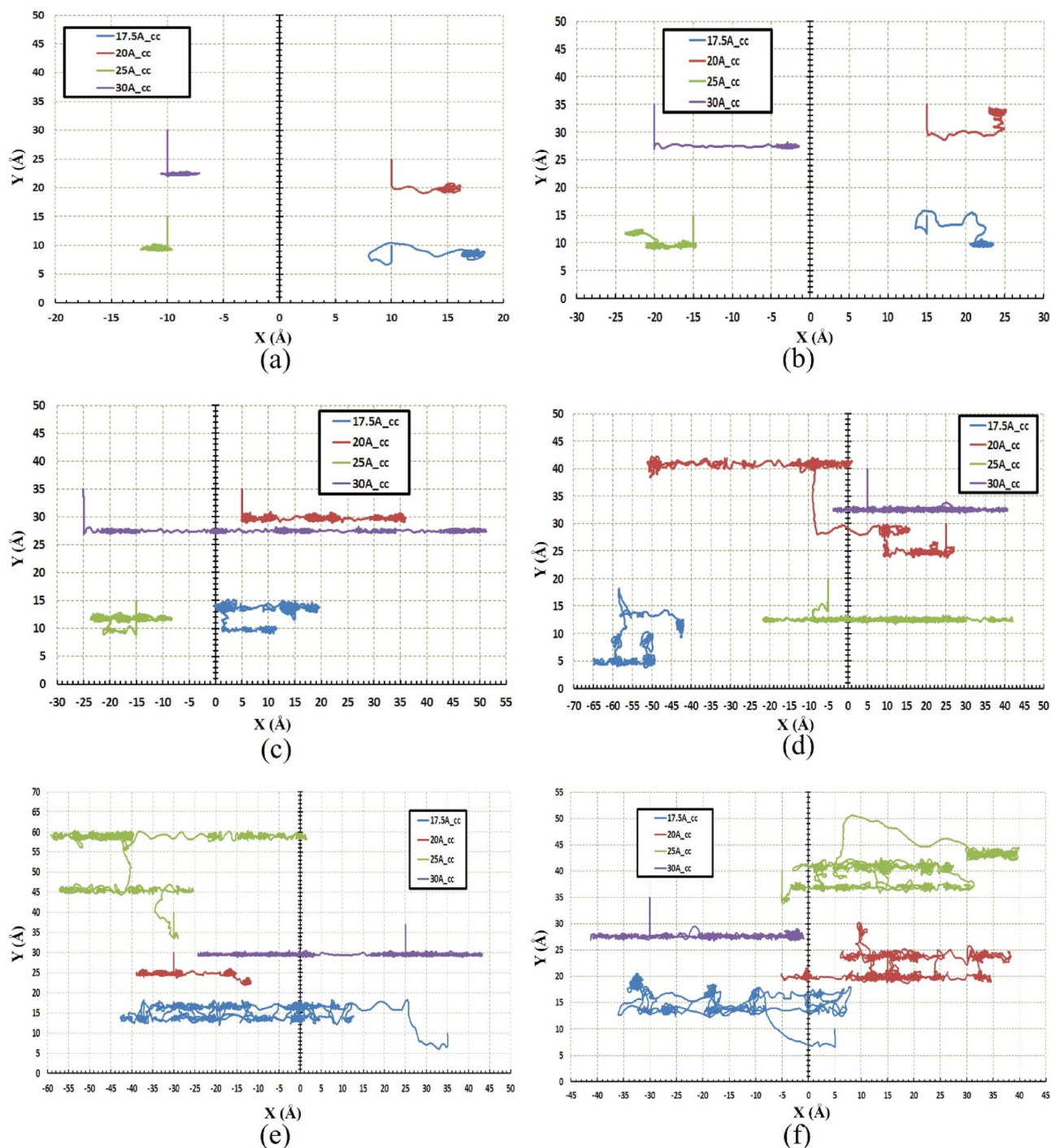


Figure 5. Trajectories of the C_{60} on the concave (cc) gold substrates during simulations (a) 75 K, (b) 150 K, (c) 300 K, (d) 400 K, (e) 500 K, and (f) 600 K. The initial deviation of the molecule at the beginning of the movement was because of adsorption towards the edges (due to the high surface-to-volume ratio).

diffusion coefficient leads to more mobility for C_{60} molecules. The maximum distance has been taken related to the radius of 20 Å at 400 K in the concave substrate and the radius of 25 Å at 600 K in the cylindrical substrate, which corresponds to the highest diffusion coefficient in each geometry. Furthermore, according to the previous studies, for a diffusion coefficient higher than $0.01 \left(\frac{\text{Å}^2}{\text{ps}}\right)$, the C_{60} molecule is able to move, but for smaller values, the molecule moves fluctuating or stationary⁵⁴. Similarly, in the current study, in both geometry at almost all temperatures and radii, the diffusion coefficient is higher than $0.01 \left(\frac{\text{Å}^2}{\text{ps}}\right)$ (Fig. 9), and the C_{60} molecule traveled a long-range distance properly. Therefore, the geometries studied in this research can be introduced as optimal geometries for C_{60} molecule. The types of C_{60} motion on different geometries were also summarized in Table S1.

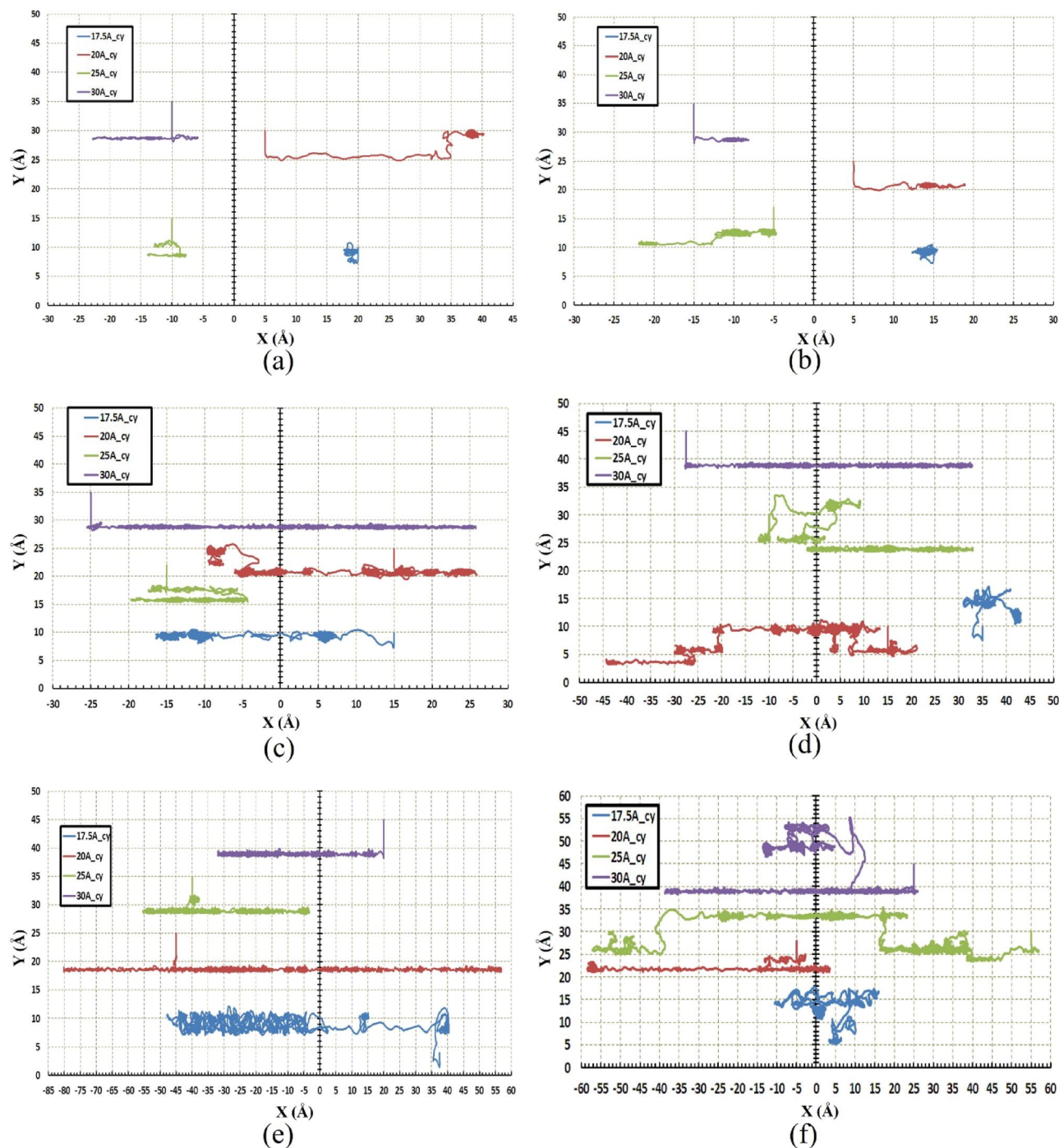


Figure 6. Trajectories of the C₆₀ on the cylindrical (cy) gold substrates during simulations (a) 75 K, (b) 150 K, (c) 300 K, (d) 400 K, (e) 500 K, and (f) 600 K. At this geometry, there is no energetic point (the points with a high surface to volume ratio), so molecule movement deviation at cylindrical substrates is lower than the concave substrates.

Nanocar. In the beginning, the regime of motion of the nanocar on the different geometries considering a range of temperature and radii is shown in Fig. 10. As mentioned in the analysis of the C₆₀ molecule, it has demonstrated long-range movement even at low temperatures due to the high diffusion coefficient. Likewise, long-range movement of nanocar at low temperature can also be observed, especially at larger radii (Fig. 10a,b). Additionally, nanocar shows non-deflection motion in the radius of 20 Å on the cylindrical substrate, which increases with the temperature significantly (Fig. 10).

Figure 11a represents the diffusion coefficient of nanocar at different temperatures and different radii for the concave substrate. It can be observed that in the lower radius (20 Å), the nanocar does not move properly so much such that it merely fluctuates along a certain length. This reciprocating movement of nanocar stems

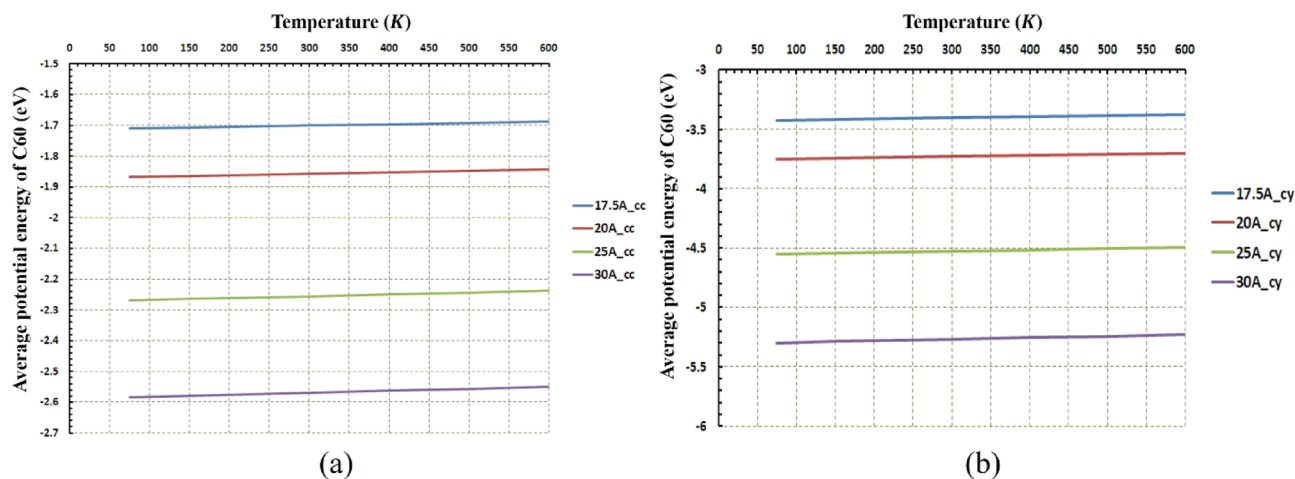


Figure 7. The average potential energy of C60 at different temperatures and radii (a) for the concave (cc) gold substrates and (b) for the cylindrical (cy) gold substrates. The temperature does not affect the average potential energy for both geometries. In cylindrical geometry, the molecule potential energy is double lower than the concave geometry.

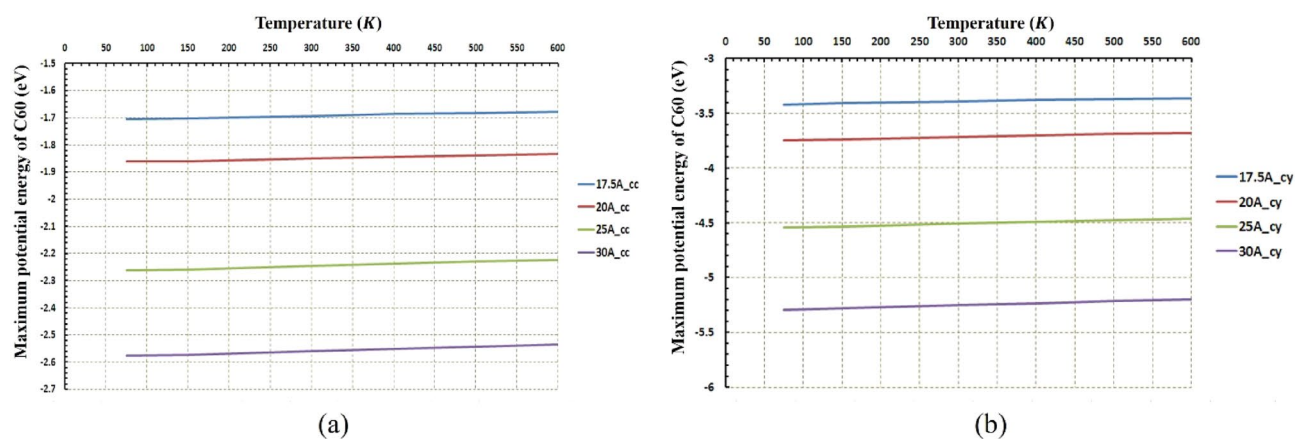


Figure 8. The Maximum potential energy of C60 at different temperatures and radii (a) for the concave (cc) gold substrates and (b) for the cylindrical (cy) gold substrates. The temperature does not affect the maximum potential energy for both geometries. In cylindrical geometry, the molecule's maximum energy is double lower than the concave geometry.

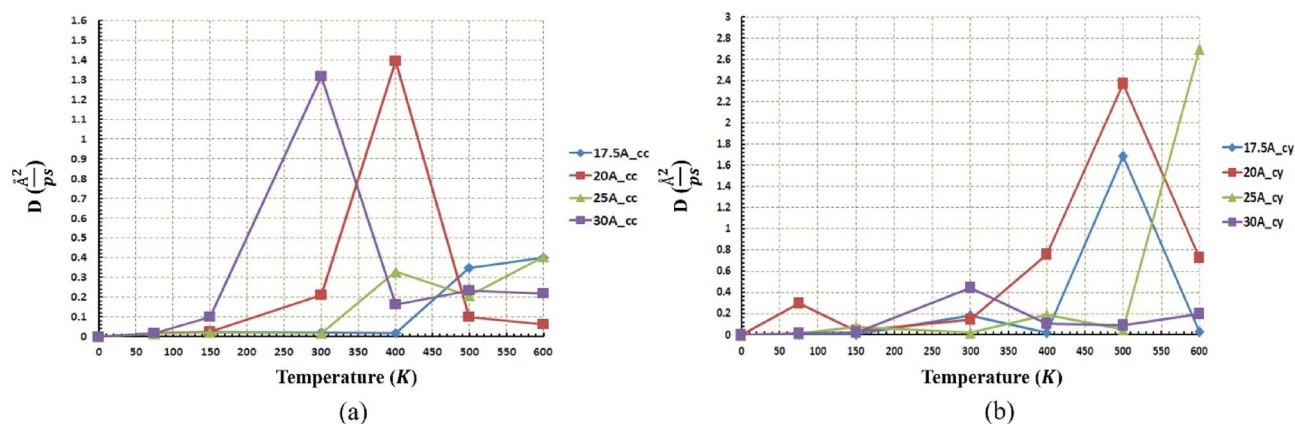


Figure 9. Diffusion coefficient of the C60 at different temperatures and radii (a) for the concave (cc) gold substrates and (b) for the cylindrical (cy) gold substrates. The diffusion coefficient at almost all radii in both geometries is higher than $0.01(\frac{\text{\AA}^2}{\text{ps}})$. That is the main reason for the long-range movement of C60.

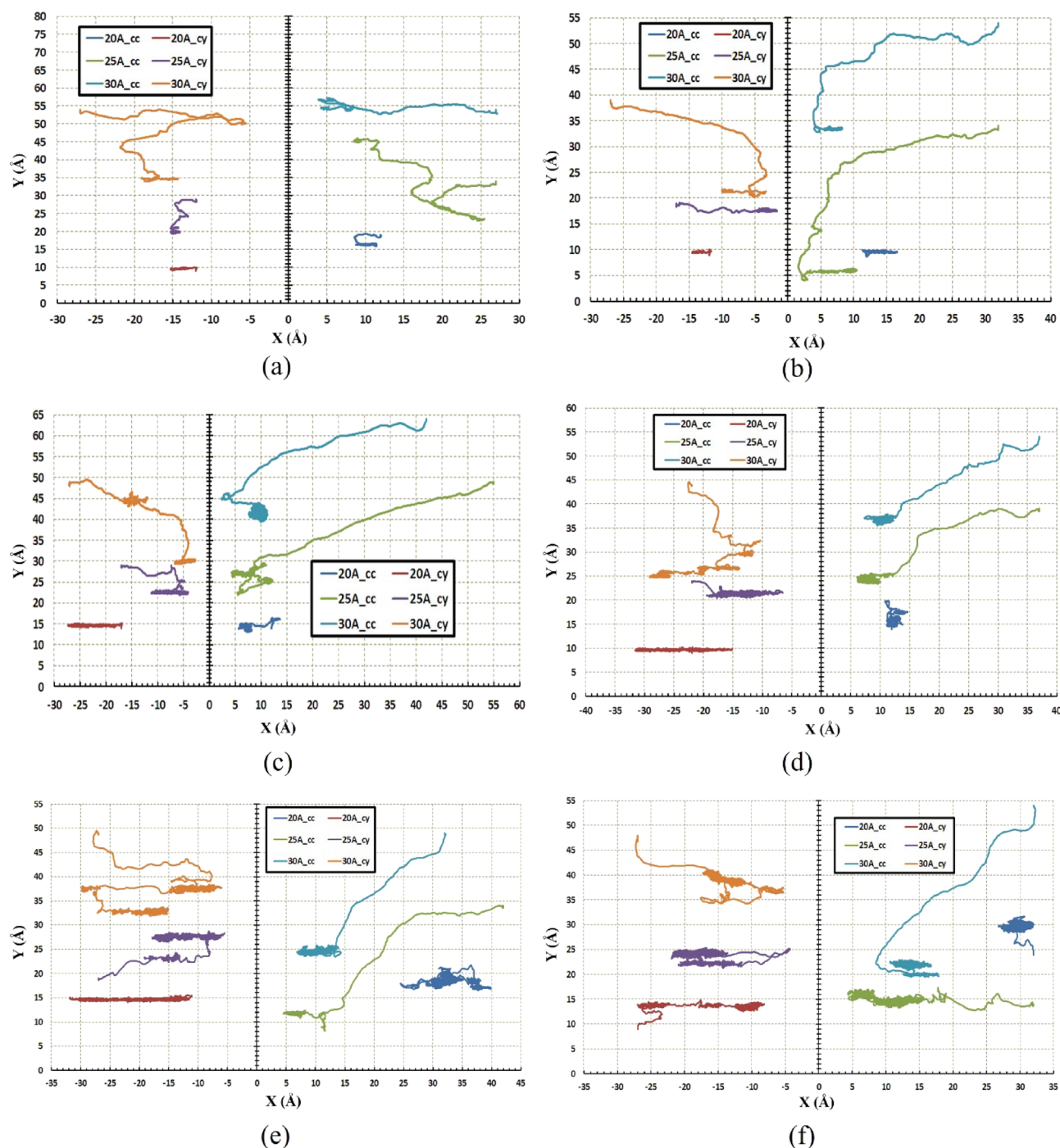


Figure 10. Trajectories of the nanocar on the concave (cc) and the cylindrical (cy) substrates during simulations (a) 75 K, (b) 150 K, (c) 300 K, (d) 400 K, (e) 500 K, and (f) 600 K. For the radius of 30 Å at both geometries and the radius of 25 Å at concave geometry, nanocar has long-range movement even at low temperatures like 75 K and 150 K.

from the small amount of diffusion coefficient in the small radii. However, in the higher radii (25 Å and 30 Å), a long-range motion of nanocars has been observed due to the higher diffusion coefficient ($DC > 0.01 \left(\frac{\text{Å}^2}{\text{ps}}\right)$).

In the large concave substrates (25 Å and 30 Å), the diffusion coefficient was greater than $0.01 \left(\frac{\text{Å}^2}{\text{ps}}\right)$ even at low temperatures (Fig. 11a). This characteristic makes them capable of being advantageous in quite a few objectives at low temperatures. In cylindrical geometry, the mentioned feature can be expressed only for radius 30 Å, according to Fig. 11b.

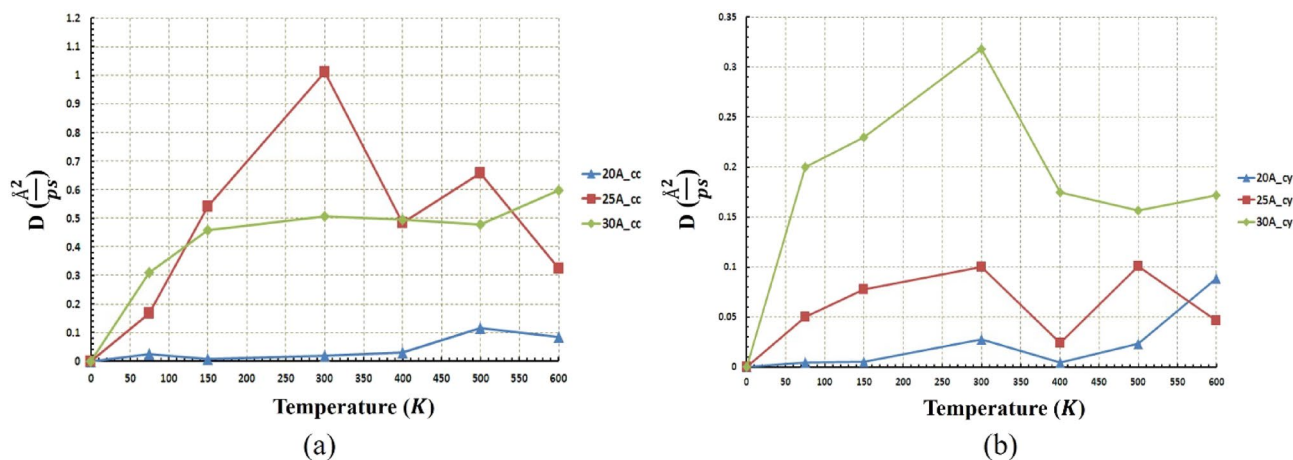


Figure 11. Diffusion coefficient of the nanocar at different temperatures and radii (a) for the concave (cc) substrates and (b) for the cylindrical (cy) substrates. The diffusion coefficient in concave geometry for almost all radii is higher than 0.01 ($\frac{\text{\AA}^2}{\text{ps}}$), but for cylindrical geometry only for the radius of 30 \AA , the diffusion coefficient is higher than 0.01 ($\frac{\text{\AA}^2}{\text{ps}}$).

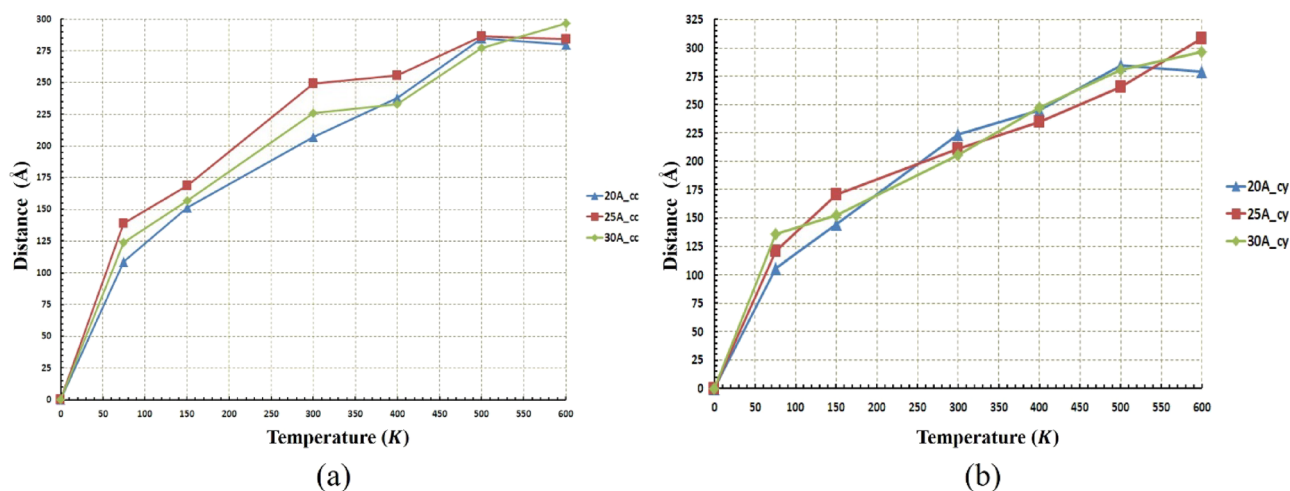


Figure 12. Distance traveled by the nanocar at different temperatures and radii (a) for the concave (cc) substrates and (b) for the cylindrical (cy) substrates. The shape of the geometry and the radius do not affect the nanocar's distance traveled. Therefore, at the same temperature, the distance traveled by nanocar in both geometries and any radius is identical.

Moreover, nanocar deviates less in the cylindrical than the concave substrate in almost all temperatures and radii. This case mainly stems from the fact that the concave substrate has a higher surface-to-volume ratio than the cylindrical substrate, which absorb the nanocar to energetic points where the surface effects are much stronger. However, a longer distance has been taken by nanocar in the concave substrate in light of the nanocar flexible chassis. Actually, in the concave substrate, the chassis has more maneuvering space and only interacts with one surface, while in the cylindrical substrate, interaction occurs from both sides. Therefore, nanocar and its chassis demonstrate better movement in concave geometry.

As mentioned before, the regime of motion of nanocar is not only temperature-dependent, but affected by radius changes as well. This issue and its relationship with the diffusion coefficient were revealed in Figs. 10 and 11. In the next stage, for more precise investigation, the movement of nanocar in different conditions is shown in Figs. 12 and 13, representing the path length and the displacement diagrams of nanocar, respectively. For better understanding about nanocar's motion, the average velocity of nanocar has been demonstrated in Fig. S1.

The equal distances have been traveled by nanocar in both substrates considering the same radii and temperatures (Fig. 12). In both geometries and for all radii, with increasing temperature, an ascending trend was observed for the distance traveled by nanocar. However, in both geometries, the effect of the radius is clearly significant, so much such that it cannot be demonstrated that increasing or decreasing the value of radius at different temperatures leads to the same trend for distance traveled by nanocar.

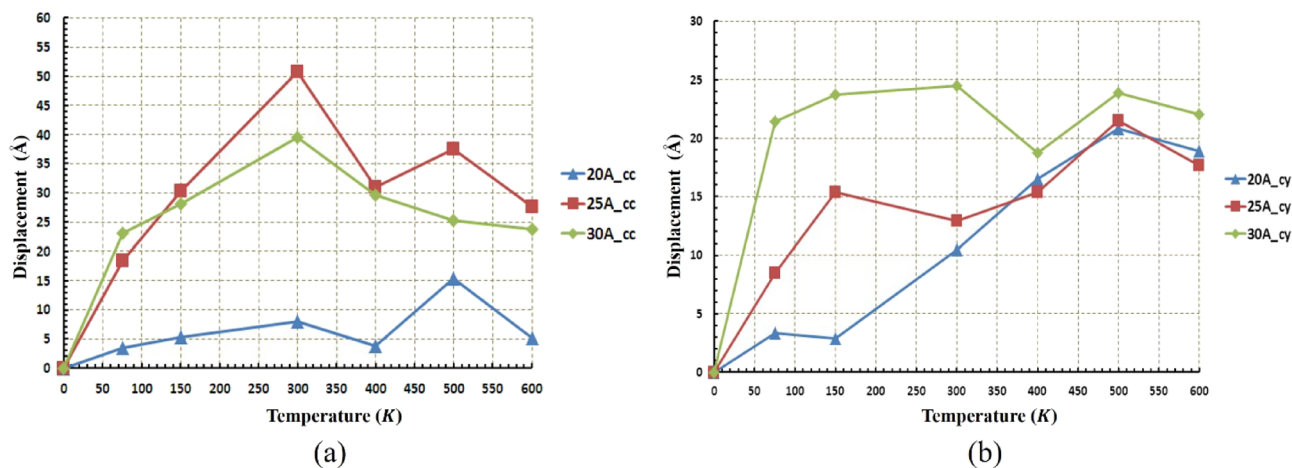


Figure 13. Displacement of the nanocar at different temperatures and radii (a) for the concave (cc) substrates (b) for the cylindrical (cy) substrates. The average displacement in concave geometry is higher than the cylindrical geometry. The maximum displacement of nanocar has occurred in the radius of 25 Å concave substrates and at 300 K.

As mentioned before, for a radius of 20 Å in concave geometry, the value of the diffusion coefficient of the nanocar is less than $0.01 \left(\frac{\text{Å}^2}{\text{ps}} \right)$ (Fig. 11a), which results in fluctuating motion of the nanocar in these conditions. By considering Figs. 12 and 13 simultaneously, a better understanding of the deviations and fluctuations above can be obtained at different conditions for the nanocar. With increasing radius in concave geometry, the diffusion coefficient increased significantly (Fig. 11a), and consequently, long-range movements of nanocar have been observed, specified in Fig. 13a. In concave geometry, maximum displacement was denoted to the radii of 25 Å, in which the greatest displacement was observed at the 300 K (Fig. 13a). Important to note this maximum displacement corresponds to the highest diffusion coefficient of nanocar in concave geometry (Fig. 11a).

In cylindrical geometry, at low temperatures in the radius of 20 Å, the fluctuating motion of nanocar occurred, and no suitable displacement was observed. In addition, increasing the temperature leads to a higher diffusion coefficient (Fig. 11b), which provides a long-range displacement for nanocar (Fig. 13b).

In the other two radii of this geometry (25 Å and 30 Å), long-range displacements were observed from the beginning (Fig. 13b). By increasing the radius, the amount of displacement has been increased at different temperatures so that in the radius of 30 Å, the nanocar has the highest displacement at all temperatures (Fig. 13b). In this radius, the maximum displacement was observed at 300 K, corresponding to the highest nanocar diffusion coefficient in cylindrical geometry (Figs. 11b and 13b). The types of C_{60} motion on different geometries were also summarized in Table S1. The types of nanocar motion on different geometries were also summarized in Table S2.

Nanotruck. Figure 14 represents graphs of nanotruck movement on the cylindrical and concave substrates. Unlike C_{60} and nanocar, which display long-range displacements, a fluctuating and indirect motion has been observed for nanotruck on both geometries at almost all temperatures.

Nanotruck fluctuation is not observed only in the radius of 17.5 Å at temperatures of 500 K and 600 K in cylindrical geometry (Fig. 14e,f). In this radius, the nanotruck shows a long-range displacement as well as direct movement.

It was expected in the concave geometry, similar to nanocar, nanotruck absorb to the high-energy edge points where the surface effects are much stronger, but nanotruck shows reciprocating motion. It seems that the nanotruck energy was not sufficient to overcome this fluctuating motion. As a result, the absorption toward high-energy points does not happen unless the nanotruck goes out of its fluctuating motion.

To investigate the nanotruck motion more accurately and better analyze its behavior, diffusion coefficient diagrams of nanotruck for both geometries were illustrated in Fig. 15. nanotruck diffusion coefficient in concave geometry is located at the boundary between fluctuating and long-range motion (previously mentioned as $0.01 \left(\frac{\text{Å}^2}{\text{ps}} \right)$). This is the main reason for the fluctuating motion of nanotruck at all temperatures and radii except the radius of 17.5 Å at 500 K, which is not significant compared to nanocar travel ranges (Fig. 15a). In cylindrical geometry, except in the radius of 17.5 Å at 500 K and 600 K, the diffusion coefficient of the nanotruck remains in the fluctuation range (Fig. 15b). In addition, at high temperatures in the radius of 17.5 Å, the diffusion coefficient of the nanotruck is sufficiently large so that nanotruck could overcome its fluctuating movement (Red lines in Fig. 14e,f).

Following the process performed in the analysis of nanotruck, Figs. 16 and 17 represent the distance traveled and displacement diagrams for nanotruck, respectively. The average velocity of nanotruck has been demonstrated Fig. S2 to attain better understanding about nanotruck's motion.

Comparing the two diagrams presented in Fig. 16, the distance traveled by the nanotruck is approximately equal at the same temperature and radius in both geometries. Unlike the temperature, by radius changes, no

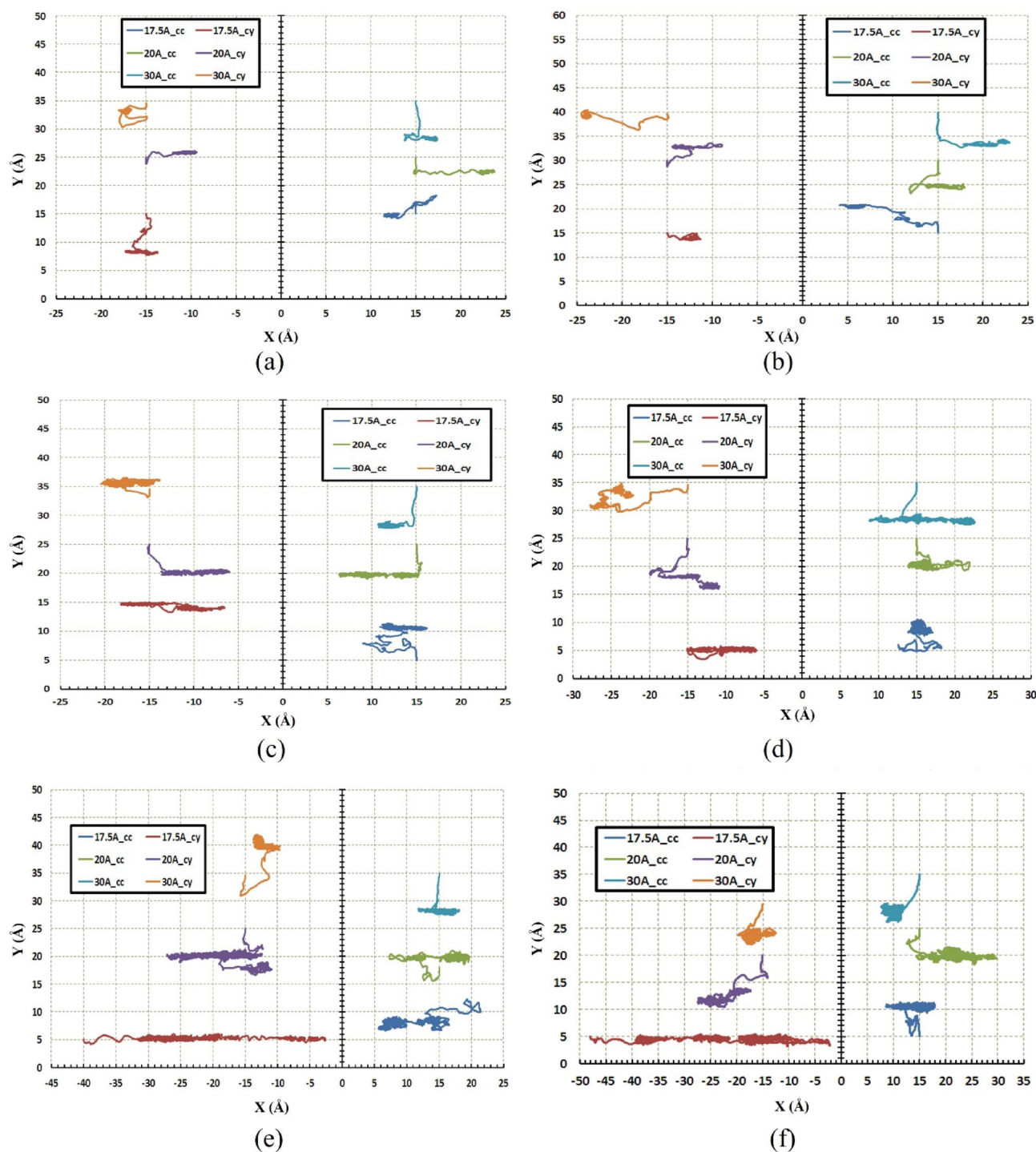


Figure 14. Trajectories of the nanotruck on the concave (cc) and the cylindrical (cy) substrates during simulations (a) 75 K, (b) 150 K, (c) 300 K, (d) 400 K, (e) 500 K, and (f) 600 K. Nanotruck has fluctuated at almost all temperatures in both geometries except the radius of 17.5 Å cylindrical substrates at 500 K and 600 K that nanotruck has long-range movement.

specific trend has been achieved since the impact of radius in different geometries is influenced by temperature changes.

The same distance has been traveled almost in all radii at 600 K and 500 K (Fig. 16b), but as mentioned earlier, due to the low diffusion coefficient in the 20 Å and 30 Å radii, the nanotruck motion remained in fluctuating range (Fig. 17b). In these two radii, despite the large distances traveled by nanotruck, short displacements have been performed by nanotruck. However, a long-range displacement was observed in the radius of 17.5 Å, which corresponds to the highest diffusion coefficient of nanotrucks in this geometry (Fig. 17b).

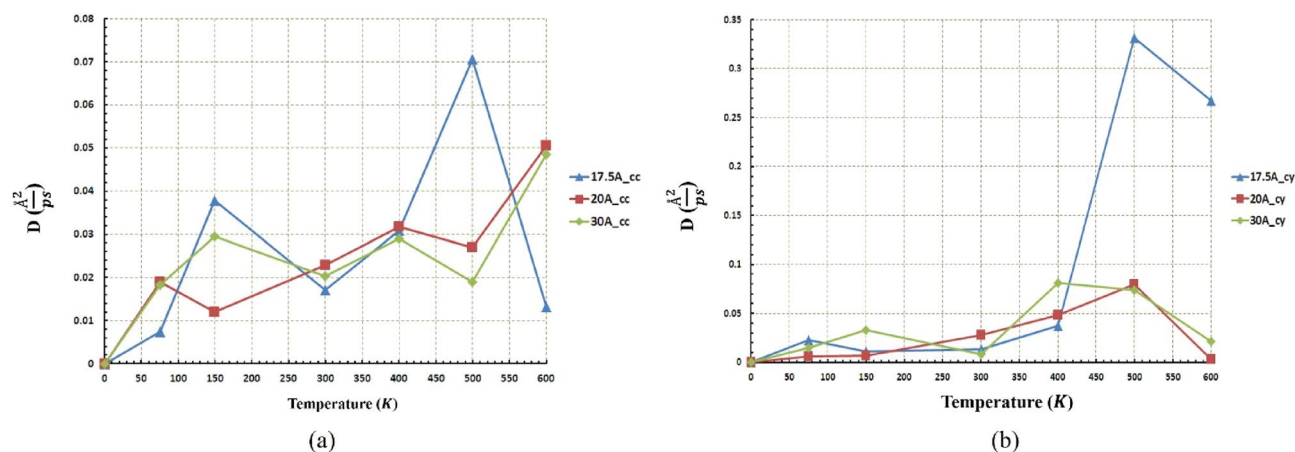


Figure 15. Diffusion coefficient of the nanotruck at different temperatures and radii (a) for the concave (cc) substrates and (b) for the cylindrical (cy) substrates. Nanotruck's diffusion coefficient in concave geometry for all radii is lower than $0.01 (\frac{\text{\AA}^2}{\text{ps}})$. In addition, nanotruck's diffusion coefficient is lower than $0.01 (\frac{\text{\AA}^2}{\text{ps}})$ in all radii except the radius of 17.5 Å at 500 K and 600 K in cylindrical geometry.

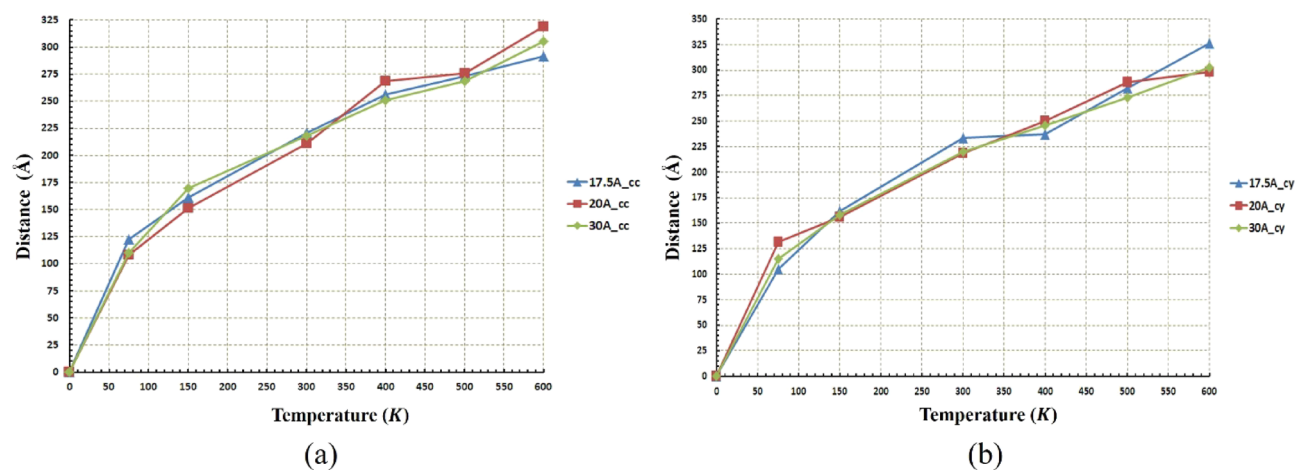


Figure 16. Distance traveled by the nanotruck at different temperatures and radii (a) for the concave (cc) substrates and (b) for the cylindrical (cy) substrates. The shape of the geometry and the radius do not affect the nanotruck's distance traveled. Hence, at the same temperature, the distance traveled by nanotruck in both geometries and any radius is identical.

Figure 17a confirms the previously presented analyzes of the fluctuating motion of nanotruck in the concave geometry. The maximum displacement of the nanotruck in concave geometry was observed at 17.5 Å, which occurred at a temperature of 600 K. It is clear that the nanotruck did not experience an excellent long-range motion in any of the simulation conditions in concave geometry in the light of the low diffusion coefficient (Figs. 15a and 17a). All in all, nanotruck, unlike C_{60} and nanocar, has not revealed acceptable performance in most conditions, except on the 17.5 Å cylindrical substrate at high temperatures. The types of nanotruck motion on different geometries were also summarized in Table S3.

Conclusion

Simulation can be a valuable tool for investigating physical/chemical phenomena^{26,50–59}. In the current project, the motion of C_{60} , nanocar, and nanotruck on the cylindrical and concave substrates, have been investigated. Considering the presented results, the deviations of C_{60} , nanocar, and nanotruck were significantly undersized compared to the previous studies³¹. This issue stems from the fact that the substrate's geometries selected in this study, restricted the non-desired directions for nano-machines. Besides, the substrate's curved shape provides a better interaction between the gold surface and C_{60} and nano-machines' wheels. The C_{60} and nanocar indicated less deviation on the cylindrical substrate than concave geometry due to fewer surface effects. In another explanation, this surface effect attracts the C_{60} and nanocar into the high-energy area (edges); thus, molecules have experienced more deviation on the concave substrate. However, since nanotruck motion was located in a small fluctuating range, the nanotruck did not absorb the high-energy area (edges). As far as potential energy is concerned, the mean and maximum potential energies were not affected by temperature changes. Therefore, this

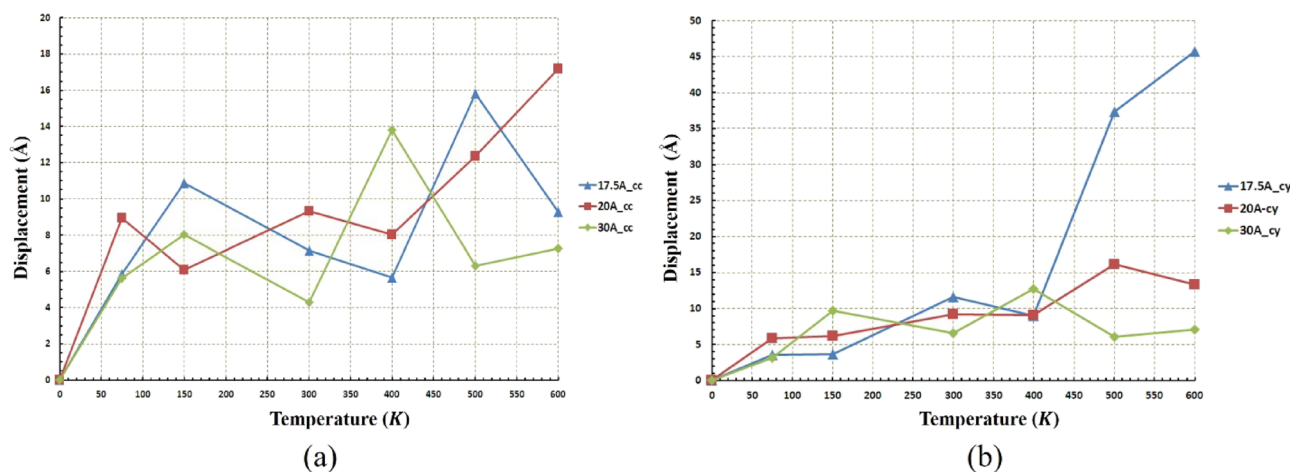


Figure 17. Displacement of the nanotruck at different temperatures and radii (a) for the concave (cc) substrates and (b) for the cylindrical (cy) substrates. Due to fluctuating movement of nanotruck in almost all conditions, the average displacement in both geometries is the same. The maximum displacement of nanotruck has occurred in the radius of 17.5 Å cylindrical substrates at 600 K.

parameter is not a cause for less mobility of C_{60} in the aforementioned items. In addition, the average and maximum potential energy were increased in the cylindrical substrate; it is twice as concave, with increasing radius in both geometries. Additionally, equal distances have been traveled by nanocar and nanotruck on both substrates considering the same radii and temperatures. In both geometries and for all radii, with increasing the temperature, an ascending trend was observed for the distance traveled by nanocar. However, in both geometries, the effect of the radius is clearly significant, so much such that it cannot be demonstrated that increasing or decreasing the value of radius at different temperatures, leads to the same trend for distance traveled by nanocar. As previously mentioned, the diffusion coefficient is recognized as the leading characteristic for defining the nano-machines' motion, which is predominantly affected by the temperature. This study revealed that the diffusion coefficient is similarly influenced notably by substrates' geometry (radius). Nonetheless, changing the radius did not specify a particular trend for the diffusion coefficient. As a result, considering the obtained radii for this study, long-range motion can be reached for nano-machines even at low temperatures (75 K or 150 K). The motion of the nanotruck on the smallest cylindrical geometry was acceptably in a direct path at high temperatures. As a result, using nanotruck in the applications, which were carried out at high temperatures (500 K to 600 K), is strongly recommended. In addition, employing the nanocar on all cylindrical substrates stated in this study is suggested extensively due to its sufficient diffusion coefficient ($DC \ll 0.01 \left(\frac{\text{Å}^2}{\text{ps}} \right)$).

Data availability

The data of this study is available upon reasonable request from the corresponding author.

Received: 2 June 2022; Accepted: 17 October 2022

Published online: 29 October 2022

References

- Murali, N., Rainu, S. K., Singh, N. & Betal, S. Advanced materials and processes for magnetically driven micro- and nano-machines for biomedical application. *Biosens. Bioelectron.* **X** 11, 100206. <https://doi.org/10.1016/j.biosx.2022.100206> (2022).
- Sitti, M. Micro- and nano-scale robotics. In *Proceedings of the 2004 American Control Conference*, vol. 1, 1–8 (2004) <https://doi.org/10.23919/ACC.2004.1383571>.
- Gorelik, R., Asaduzzaman, A., Manga, V. R., Thakur, A. & Muralidharan, K. A first-principles investigation of lithium and sodium ion diffusion in C_{60} molecular solids. *J. Phys. Chem. C* **126**(9), 4259–4266. <https://doi.org/10.1021/acs.jpcc.1c09269> (2022).
- Karan, S. & Majumder, D. D. Molecular machinery—a nanorobotics control system design for cancer drug delivery. In *2011 International Conference on Recent Trends in Information Systems*, 197–202 (2011) <https://doi.org/10.1109/ReTIS.2011.6146867>.
- Mahboobi, S. H., Meghdari, A., Jalili, N. & Amiri, F. Qualitative study of nanocluster positioning process: Planar molecular dynamics simulations. *Curr. Appl. Phys.* **9**(5), 997–1004. <https://doi.org/10.1016/j.cap.2008.10.006> (2009).
- Cuberes, M. T., Schlittler, R. R. & Gimzewski, J. K. Room-temperature repositioning of individual C_{60} molecules at Cu steps: Operation of a molecular counting device. *Appl. Phys. Lett.* **69**(20), 3016–3018. <https://doi.org/10.1063/1.116824> (1996).
- Sziklai, D. *et al.* Nanosurgical manipulation of titin and its m-complex. *Nanomaterials* **12**(2), 178. <https://doi.org/10.3390/nano12020178> (2022).
- Sasaki, T., Morin, J.-F., Lu, M. & Tour, J. M. Synthesis of a single-molecule nanotruck. *Tetrahedron Lett.* **48**(33), 5817–5820. <https://doi.org/10.1016/j.tetlet.2007.06.081> (2007).
- Vives, G. & Tour, J. M. Synthesis of single-molecule nanocars. *Acc. Chem. Res.* **42**(3), 473–487. <https://doi.org/10.1021/ar8002317> (2009).
- Kinbara, K. & Aida, T. Toward intelligent molecular machines: Directed motions of biological and artificial molecules and assemblies. *Chem. Rev.* **105**(4), 1377–1400. <https://doi.org/10.1021/cr030071r> (2005).
- Popov, V. L. Nanomachines: Methods to induce a directed motion at nanoscale. *Phys. Rev. E* **68**(2), 026608. <https://doi.org/10.1103/PhysRevE.68.026608> (2003).

12. Shirai, Y. *et al.* Surface-rolling molecules. *J. Am. Chem. Soc.* **128**(14), 4854–4864. <https://doi.org/10.1021/ja058514r> (2006).
13. Zhang, J. *et al.* Investigating the motion of molecular machines on surfaces by STM: The nanocar and beyond. In *2007 7th IEEE Conference on Nanotechnology (IEEE NANO)*, 243–246 (2007) <https://doi.org/10.1109/NANO.2007.4601180>.
14. Sasaki, T., Osgood, A. J., Alemany, L. B., Kelly, K. F. & Tour, J. M. Synthesis of a nanocar with an angled chassis. Toward circling movement. *Org. Lett.* **10**(2), 229–232. <https://doi.org/10.1021/ol702642r> (2008).
15. Sasaki, T. & Tour, J. M. Synthesis of a dipolar nanocar. *Tetrahedron Lett.* **48**(33), 5821–5824. <https://doi.org/10.1016/j.tetlet.2007.06.080> (2007).
16. Morin, J.-F., Sasaki, T., Shirai, Y., Guerrero, J. M. & Tour, J. M. Synthetic routes toward carborane-wheeled nanocars. *J. Org. Chem.* **72**(25), 9481–9490. <https://doi.org/10.1021/jo701400t> (2007).
17. Lohrasebi, A., Neek-Amal, M. & Ejtehadi, M. R. Directed motion of C60 on a graphene sheet subjected to a temperature gradient. *Phys. Rev. E* **83**(4), 042601. <https://doi.org/10.1103/PhysRevE.83.042601> (2011).
18. Shamloo, A., Bakhtiari, M. A., Tohidloo, M. & Seifi, S. Investigation of fullerene motion on thermally activated gold substrates with different shapes. *Sci. Rep.* **12**(1), 14397. <https://doi.org/10.1038/s41598-022-18730-7> (2022).
19. Pinardi, A. L. *et al.* Vacancy formation on C60/Pt (111): Unraveling the complex atomistic mechanism. *Nanotechnology* **25**(38), 385602. <https://doi.org/10.1088/0957-4484/25/38/385602> (2014).
20. Wang, L.-L. & Cheng, H.-P. Rotation, translation, charge transfer, and electronic structure of C60 on Cu(111) surface. *Phys. Rev. B* **69**(4), 045404. <https://doi.org/10.1103/PhysRevB.69.045404> (2004).
21. Kelly, K. Probing molecular machines on surfaces: The nanocar and beyond. *Microsc. Microanal.* **14**(S2), 956–957. <https://doi.org/10.1017/S1431927608085176> (2008).
22. Shirai, Y., Osgood, A. J., Zhao, Y., Kelly, K. F. & Tour, J. M. Directional control in thermally driven single-molecule nanocars. *Nano Lett.* **5**(11), 2330–2334. <https://doi.org/10.1021/nl051915k> (2005).
23. Grill, L. ChemInform abstract: Functionalized molecules studied by STM: Motion, switching and reactivity. *ChemInform* <https://doi.org/10.1002/chin.200823260> (2008).
24. Nejat Pishkenari, H., Nemati, A., Meghdari, A. & Sohrabpour, S. A close look at the motion of C60 on gold. *Curr. Appl. Phys.* **15**(11), 1402–1411. <https://doi.org/10.1016/j.cap.2015.08.003> (2015).
25. Mofidi, S. M., Nejat Pishkenari, H., Ejtehadi, M. R. & Akimov, A. V. Locomotion of the C60-based nanomachines on graphene surfaces. *Sci. Rep.* **11**(1), 2576. <https://doi.org/10.1038/s41598-021-82280-7> (2021).
26. Shamloo, A., Mohammadaliha, N. & Mohseni, M. Integrative utilization of microenvironments, biomaterials and computational techniques for advanced tissue engineering. *J. Biotechnol.* **212**, 71–89. <https://doi.org/10.1016/j.jbiotec.2015.08.005> (2015).
27. Shamloo, A., Nejad, M. A. & Saeedi, M. Fluid–structure interaction simulation of a cerebral aneurysm: Effects of endovascular coiling treatment and aneurysm wall thickening. *J. Mech. Behav. Biomed. Mater.* **74**, 72–83. <https://doi.org/10.1016/j.jmbbm.2017.05.020> (2017).
28. Akimov, A. V., Nemukhin, A. V., Moskovsky, A. A., Kolomeisky, A. B. & Tour, J. M. Molecular dynamics of surface-moving thermally driven nanocars. *J. Chem. Theory Comput.* **4**(4), 652–656. <https://doi.org/10.1021/ct7002594> (2008).
29. Konyukhov, S. S. *et al.* Rigid-body molecular dynamics of fullerene-based nanocars on metallic surfaces. *J. Chem. Theory Comput.* **6**(9), 2581–2590. <https://doi.org/10.1021/ct100101y> (2010).
30. Konyukhov, S. S. *et al.* Diffusion of fullerene-based nanocars on the surface of a gold crystal. *Moscow Univ. Chem. Bull.* **65**(4), 219–220. <https://doi.org/10.3103/S0027131410040012> (2010).
31. Nemati, A., Nejat Pishkenari, H., Meghdari, A. & Sohrabpour, S. Directing the diffusive motion of fullerene-based nanocars using nonplanar gold surfaces. *Phys. Chem. Chem. Phys.* **20**(1), 332–344. <https://doi.org/10.1039/C7CP07217A> (2018).
32. Liu, Y., Zhu, J., Weng, G., Li, J. & Zhao, J. Gold nanotubes: Synthesis, properties and biomedical applications. *Microchim. Acta* **187**(11), 612. <https://doi.org/10.1007/s00604-020-04460-y> (2020).
33. Bilalbegović, G. Gold nanotube: Structure and melting. *Vacuum* **71**(1–2), 165–169. [https://doi.org/10.1016/S0042-207X\(02\)00732-7](https://doi.org/10.1016/S0042-207X(02)00732-7) (2003).
34. Shamraiz, U. *et al.* Gold nanotubes and nanorings: Promising candidates for multidisciplinary fields. *Int. Mater. Rev.* **64**(8), 478–512. <https://doi.org/10.1080/09506608.2018.1554991> (2019).
35. Chao, C. H., Ju, S. P., Weng, M. H., Lee, W. J. & Hsieh, N. K. Simulation of water molecules inside gold nanotubes of various sizes and temperatures. *J. Nanosci. Nanotechnol.* **9**(2), 880–884. <https://doi.org/10.1166/jnn.2009.C045> (2009).
36. Dereli, G., Süngü, B. & Özdoğan, C. Thermal stability of metallic single-walled carbon nanotubes: An O(N) tight-binding molecular dynamics simulation study. *Nanotechnology* **18**(24), 245704. <https://doi.org/10.1088/0957-4484/18/24/245704> (2007).
37. Wang, J. *et al.* Melting behavior in ultrathin metallic nanowires. *Phys. Rev. B* **66**(8), 085408. <https://doi.org/10.1103/PhysRevB.66.085408> (2002).
38. Dutta, B. N. & Dayal, B. Lattice constants and thermal expansion of gold up to 878 °C by X-ray method. *Phys. Status Solidi* **3**(3), 473–477. <https://doi.org/10.1002/pssb.19630030312> (1963).
39. Foiles, S. M., Baskes, M. I. & Daw, M. S. Embedded-atom-method functions for the fcc metals Cu, Ag, Au, Ni, Pd, Pt, and their alloys. *Phys. Rev. B* **33**(12), 7983–7991. <https://doi.org/10.1103/PhysRevB.33.7983> (1986).
40. Daw, M. S. & Baskes, M. I. Embedded-atom method: Derivation and application to impurities, surfaces, and other defects in metals. *Phys. Rev. B* **29**(12), 6443–6453. <https://doi.org/10.1103/PhysRevB.29.6443> (1984).
41. Stukowski, A., Sadigh, B., Erhart, P. & Caro, A. Efficient implementation of the concentration-dependent embedded atom method for molecular-dynamics and Monte-Carlo simulations. *Model. Simul. Mater. Sci. Eng.* **17**(7), 075005. <https://doi.org/10.1088/0965-0393/17/7/075005> (2009).
42. Watkins, E. K. & Jorgensen, W. L. Perfluoroalkanes: Conformational analysis and liquid-state properties from ab initio and Monte Carlo calculations. *J. Phys. Chem. A* **105**(16), 4118–4125. <https://doi.org/10.1021/jp004071w> (2001).
43. Allinger, N. L. Conformational analysis. 130. MM2. A hydrocarbon force field utilizing V1 and V2 torsional terms. *J. Am. Chem. Soc.* **99**(25), 8127–8134. <https://doi.org/10.1021/ja00467a001> (1977).
44. Allinger, N. L., Chen, K. & Lii, J.-H. An improved force field (MM4) for saturated hydrocarbons. *J. Comput. Chem.* **17**(5–6), 642–668. [https://doi.org/10.1002/\(SICI\)1096-987X\(199604\)17:5<63c642::AID-JCC6%3e3.0.CO;2-U](https://doi.org/10.1002/(SICI)1096-987X(199604)17:5<63c642::AID-JCC6%3e3.0.CO;2-U) (1996).
45. Allinger, N. L., Yuh, Y. H. & Lii, J. H. Molecular mechanics. The MM3 force field for hydrocarbons. 1. *J. Am. Chem. Soc.* **111**(23), 8551–8566. <https://doi.org/10.1021/ja00205a001> (1989).
46. Lii, J. H. & Allinger, N. L. Molecular mechanics. The MM3 force field for hydrocarbons. 3. The van der Waals' potentials and crystal data for aliphatic and aromatic hydrocarbons. *J. Am. Chem. Soc.* **111**(23), 8576–8582. <https://doi.org/10.1021/ja00205a003> (1989).
47. Lii, J. H. & Allinger, N. L. Molecular mechanics. The MM3 force field for hydrocarbons. 2. Vibrational frequencies and thermodynamics. *J. Am. Chem. Soc.* **111**(23), 8566–8575. <https://doi.org/10.1021/ja00205a002> (1989).
48. Plimpton, S. Fast parallel algorithms for short-range molecular dynamics. *J. Comput. Phys.* **117**(1), 1–19. <https://doi.org/10.1006/jcph.1995.1039> (1995).
49. Humphrey, W., Dalke, A. & Schulten, K. VMD: Visual molecular dynamics. *J. Mol. Graph.* **14**(1), 33–38. [https://doi.org/10.1016/0263-7855\(96\)00018-5](https://doi.org/10.1016/0263-7855(96)00018-5) (1996).
50. Valiev, M. *et al.* NWChem: A comprehensive and scalable open-source solution for large scale molecular simulations. *Comput. Phys. Commun.* **181**(9), 1477–1489. <https://doi.org/10.1016/j.cpc.2010.04.018> (2010).
51. Akimov, A. V. & Kolomeisky, A. B. Unidirectional rolling motion of nanocars induced by electric field. *J. Phys. Chem. C* **116**(42), 22595–22601. <https://doi.org/10.1021/jp306938b> (2012).

52. Nemati, A., Pishkenari, H. N., Meghdari, A. & Shorabpour, S. Nanocar & nanotruck motion on gold surface. In *2016 International Conference on Manipulation, Automation and Robotics at Small Scales (MARSS)*, 1–6 (2016) <https://doi.org/10.1109/MARSS.2016.7561699>.
53. Heinz, H., Vaia, R. A., Farmer, B. L. & Naik, R. R. Accurate simulation of surfaces and interfaces of face-centered cubic metals using 12–6 and 9–6 Lennard-Jones potentials. *J. Phys. Chem. C* **112**(44), 17281–17290. <https://doi.org/10.1021/jp801931d> (2008).
54. Nemati, A., Meghdari, A., Nejat Pishkenari, H. & Sohrabpour, S. Investigation into thermally activated migration of fullerene-based nanocars. *Sci. Iran.* <https://doi.org/10.24200/sci.2018.20321> (2018).
55. Manzoori, A., Fallah, F., Sharzehee, M. & Ebrahimi, S. Computational investigation of the stability of stenotic carotid artery under pulsatile blood flow using a fluid-structure interaction approach. *Int. J. Appl. Mech.* **12**(10), 2050110. <https://doi.org/10.1142/S1758825120501100> (2020).
56. Biglari, H., Razaghi, R., Ebrahimi, S. & Karimi, A. A computational dynamic finite element simulation of the thoracic vertebrae under blunt loading: Spinal cord injury. *J. Brazil. Soc. Mech. Sci. Eng.* **41**(2), 84. <https://doi.org/10.1007/s40430-019-1588-z> (2019).
57. Alishiri, M., Ebrahimi, S., Shamloo, A., Boroumand, A. & Mofrad, M. R. K. Drug delivery and adhesion of magnetic nanoparticles coated nanoliposomes and microbubbles to atherosclerotic plaques under magnetic and ultrasound fields. *Eng. Appl. Comput. Fluid Mech.* **15**(1), 1703–1725. <https://doi.org/10.1080/19942060.2021.1989042> (2021).
58. Ebrahimi, S. & Fallah, F. Investigation of coronary artery tortuosity with atherosclerosis: A study on predicting plaque rupture and progression. *Int. J. Mech. Sci.* **223**, 107295. <https://doi.org/10.1016/j.ijmecsci.2022.107295> (2022).
59. Shamloo, A., Pedram, M. Z., Heidari, H. & Alasty, A. Computing the blood brain barrier (BBB) diffusion coefficient: A molecular dynamics approach. *J. Magn. Magn. Mater.* **410**, 187–197. <https://doi.org/10.1016/j.jmmm.2016.03.030> (2016).

Acknowledgements

This research did not receive any specific grant from funding agencies in the public, commercial, or not-for-profit sectors.

Author contributions

M.A.B. designed the simulations, performed the simulations and wrote the paper. S.S. designed the simulations, performed the simulations and wrote the paper. M.T. designed the simulations, performed the simulations and wrote the paper. A.S. designed the simulations, supervised the study and wrote the paper.

Competing interests

The authors declare no competing interests.

Additional information

Supplementary Information The online version contains supplementary material available at <https://doi.org/10.1038/s41598-022-22517-1>.

Correspondence and requests for materials should be addressed to A.S.

Reprints and permissions information is available at www.nature.com/reprints.

Publisher's note Springer Nature remains neutral with regard to jurisdictional claims in published maps and institutional affiliations.



Open Access This article is licensed under a Creative Commons Attribution 4.0 International License, which permits use, sharing, adaptation, distribution and reproduction in any medium or format, as long as you give appropriate credit to the original author(s) and the source, provide a link to the Creative Commons licence, and indicate if changes were made. The images or other third party material in this article are included in the article's Creative Commons licence, unless indicated otherwise in a credit line to the material. If material is not included in the article's Creative Commons licence and your intended use is not permitted by statutory regulation or exceeds the permitted use, you will need to obtain permission directly from the copyright holder. To view a copy of this licence, visit <http://creativecommons.org/licenses/by/4.0/>.

© The Author(s) 2022